Jalalvand, M., Hosseini-Toudeshky, H., & Mohammadi, B. (2013). Numerical modeling of diffuse transverse cracks and induced delamination using cohesive elements. *Proceedings of the Institution of Mechanical Engineers, Part C: Journal of Mechanical Engineering Science*, *227*(7), 1392-1405. https://doi.org/10.1177/0954406212460974

Numerical Modeling of Diffuse Transverse Cracks and Induced Delamination using Cohesive Elements

Meisam Jalalvand[1], Hossein Hosseini-Toudeshky[1*], and Bijan Mohammadi[2]

[1]Department of Aerospace Engineering, Amirkabir University of Technology, Hafez ave., Tehran, Iran

[2]School of Mechanical Engineering, Iran University of Science & Technology, Narmak, Tehran, Iran

Abstract

This paper is devoted to the modeling of spread kind of damages such as matrix cracking and induced delamination in symmetric and asymmetric cross-ply laminates of composite materials using cohesive elements. For matrix crack modeling, parallel rows of cohesive elements are used between every row of 2D elements in 90˚ layers. Delamination is also modeled by cohesive elements at the 90˚/0˚ interface. Since matrix cracking is a diffuse kind of damage mechanism, application of cohesive elements is not straightforward, and special techniques are necessary to resolve the modeling difficulties. For this purpose, two techniques of "*bisecting*" and "*random distribution of strength of cohesive elements*" are proposed here. Both techniques are applied to various symmetric laminates of $[0/90_3]_s$ and $[90_n/0]_s$ (n=1 to 3). The predicted stiffness and damage progresses from both techniques are in good agreement with the experimental results. Then, asymmetric cross-ply laminates of $[90_n/0]$ (n=1 to 3) are analyzed to show the capability of this method in progressive damage analyses. The proposed method is less restricted in comparison with available micromechanical methods and is able to predict damage initiation, propagation and damage-mode transition for any symmetric and asymmetric cross-ply sequence. Therefore, this method can be used for development of "in-plane damage" constitutive laws especially when specimens are subjected to complex loading and boundary conditions.

Keywords:

Diffuse damage, Transverse crack, Induced delamination, Cross-ply, Composite laminate, Cohesive element, Numerical modeling

[*] Corresponding Author, hosseini@aut.ac.ir, Tel: +98 21 6454 3224

Proc Inst Mech Eng Part C, 227(7), 1392–1405
http://pic.sagepub.com/content/227/7/1392

1) Introduction

Damage mechanisms in cross-ply laminates under longitudinal tension loading usually include transverse cracking (cracks in 90˚ layers normal to the loading direction) and delamination (separation between 90˚ and 0˚ layers). When a plain specimen is subjected to tensile loading, the first destructive event is matrix/transverse cracking. Transverse cracks accumulate up to a certain density, and then damage mechanism changes to delamination induced by transverse cracks (see Figure 1 (a)). This type of delamination initiates from the tips of matrix microcracks and propagates through the width of specimen and between the two free edges of laminate.

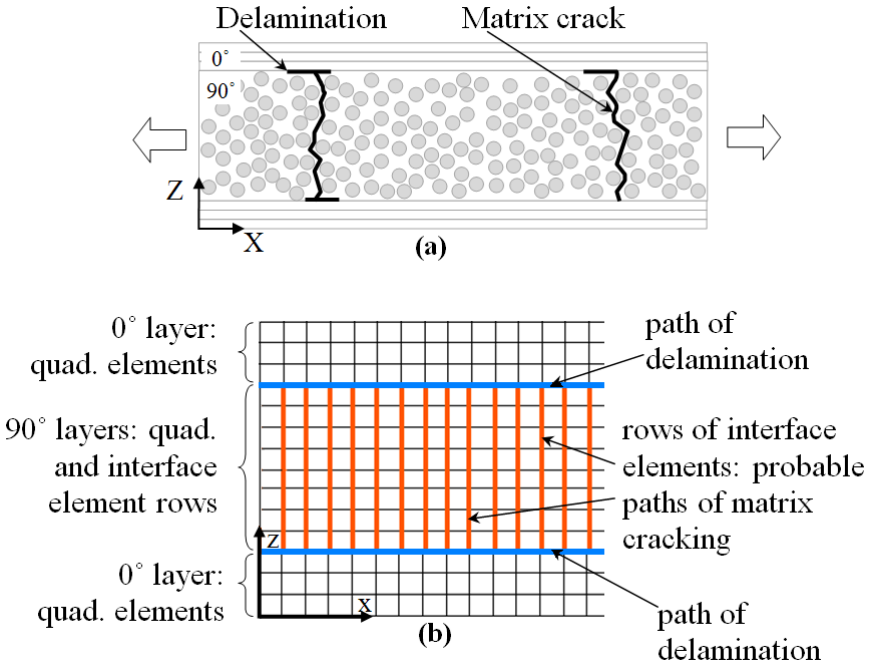

Figure 1. (a) Typical $[0/90_n]_s$ layup under tension loading, (b) 2D finite element model of $[0/90_n]_s$ layup with cohesive elements for modeling of matrix cracking and delamination

This damage phenomena has been widely addressed by micro-mechanical approaches in the literature; mostly by analytical methods [1-2] and especially by shear-lag method [3-6]. Variational technique [7-9] and finite element methods [10-11] have been generally used for deriving the stress distribution at the 90˚/0˚ interface. Each method contains specific assumptions and outcome with considerable progress in the field [12]. However, very few investigations [13] have been performed on "*numerical simulation*" of matrix cracking and induced delamination as diffuse kind of damages. One of the main issue in such kind of modeling is the unknown location and large number of matrix cracks [14], and the possibility of induced delamination which makes more complications in the numerical procedure.

On the other hand, numerical modeling of damage in composite laminates have been usually performed in macro- and meso- scaling approaches, in which the cracks are not considered as single discontinuity and the overall effects of cracking is usually modeled by continuum

damage mechanics [15]. Finite elements method has been widely used and valuable progress has been reached in proposing different types of advanced constitutive laws with different damage behaviors such as coupled damage-plasticity [16], nonlocal damage [17], and viscoelastic-damge [18].

However, it has been shown that meso-scale damage modeling of composite laminates contains many shortcomings without micro-mechanical information [19-20]. In other words, to benefit the advantage of all capabilities of macro-scale modeling, some information is required, which is merely available from micro-scale modeling. In fact, this is the reason of recent tendency to multi-scale modeling for numerical investigation of damage analyses in composite materials [21-23].

In this paper, a numerical approach using finite element method is proposed for matrix cracking and induced delamination analyses, in which different types of damages are considered as separate discontinuities similar to the micro-scale modeling. The main advantage of such method in comparison with former micro-mechanical methods is not only simulating both damage initiation and propagation, but also it's less restriction in specimen type and boundary conditions due to the application of finite element method. Furthermore, the proposed approach can be used for developing of general "*mechanism-based*" in-plane constitutive law.

2) Proposed approach

2-1) Element architecture

In micro-scale approach, matrix cracks are strong discontinuities in displacement field that may appear in the 90˚ ply groups. Due to the existence of large number of matrix cracks, they are usually known as a spread or diffuse kind of damage mechanism [24]. Therefore, the undetermined probable position and diffuse nature of them make this damage mechanism more complicated. In this paper, the authors intend to demonstrate a practical procedure to scrimmage with these difficulties using finite elements method for simulation of such phenomena.

In this investigation, cohesive elements are placed between the quadrilateral elements of 90˚ layers to predict the initiation and propagation of matrix cracks and delamination. Figure 1 (b) shows a typical $[0/90_n]_s$ lay-up and the considered cohesive elements in various rows in 90˚ layer for matrix cracking predictions and on the interfaces of 90˚ and 0˚ layers to predict the delamination initiation and growth. In this figure, the thick vertical line between the possible delamination paths shows 6-node 1D cohesive elements while the normal 8-node 2D quadrilateral elements are used for the rest domains of 0˚ and 90˚ layers. The cohesive elements with zero thickness are used in the modeling.

2-2) Elastic behavior

In a model with *m* rows of quadrilateral elements and *m-1* rows of cohesive elements which typically shown in Figure 2, accumulated deformation of cohesive elements may cause

erroneous stiffness decrease of 90˚ layers. Such an error cannot be omitted completely when conventional cohesive elements are used but it can be decreased by decreasing the number of cohesive elements and also management of proper characteristic parameters of cohesive elements. The stress components of cohesive elements can be defined as:

$$\sigma_j = K\Delta_j(1-D) \tag{1}$$

Where σ_j and Δ_j (j=1 and 2) are stress and displacement discontinuity in x and z local coordinate of cohesive element. K and D are penalty stiffness and damage parameters respectively.

When the model is under a uniaxial tension loading (Figure 2(b)), the average strain of such model is as follows:

$$\varepsilon_2 = \frac{m\Delta_q + (m-1)\Delta_i}{L} = \frac{\sigma}{E_2^*} + \frac{m-1}{L}\frac{\sigma}{K} \tag{2}$$

where E_2^* is the stiffness of an un-damaged ply in second principle direction, L is the total length of the specimen and Δ_q and Δ_i are deformation of a quadrilateral and cohesive element respectively. Easily the stiffness of the proposed model containing m-1 rows of cohesive elements can be calculated by dividing of Equation (2) by σ. So the normalized stiffness of the proposed model in Figure 2(b) with respect to the stiffness of an original layer with no cohesive elements shown in Figure 2 (c) becomes as follows:

$$\frac{E_2}{E_2^*} = \frac{1}{1+\frac{m-1}{L}\frac{E_2^*}{K}} \tag{3}$$

where E_2 is the stiffness of a 90º ply, modeled with the proposed cohesive approach. Obviously the accuracy of the modeling in the linear-elastic part of analysis would be improved when the ratio of E_2/E_2^* becomes close to unity. To maintain such condition in (3), the value of $\frac{m-1}{L}\frac{E_2^*}{K}$ should be vanished in elastic condition. Such an aim can be reached by increasing the penalty stiffness value of cohesive elements (K) and/or by decreasing the number of cohesive elements rows in a specimen with length L.

Variations of the obtained stiffness ratio, E_2/E_2^*, versus the penalty stiffness value for a specimen with length of L=6.4 mm, E^*_2=9.6E3 MPa and m=256 is compared with those obtained from plane stress and plane strain elastic finite element analyses in Figure 3. This figure shows that, for the penalty values of less than K=1.0E6 N/mm^3, the ratio of E_2/E_2^* experiences a severe drop and for more accurate results of such model, the penalty values of larger than K=1.0E7 N/mm^3 have to be chosen. In conventional numerical models with just one row of cohesive element similar to the DCB and ENF specimens, the penalty stiffness values of between K=1E5 N/mm^3 and K=1E7 N/mm^3 are usually recommended [25]. But, as

shown in Figure 3, such values may lead to erroneous elastic stiffness prediction in this kind of analysis. It should be noted that the obtained results are completely associated with the value of elastic modulus of the ply in second principle direction E^*_2. In the case of larger values of E^*_2 the penalty stiffness should be chosen even larger. The ratio of $m-1/L$ is in fact related to the density of cohesive element rows and in this proposed model, it is related to the quadrilateral element size. By reducing the number of cohesive element rows, it is possible to increase the stiffness ratio as well.

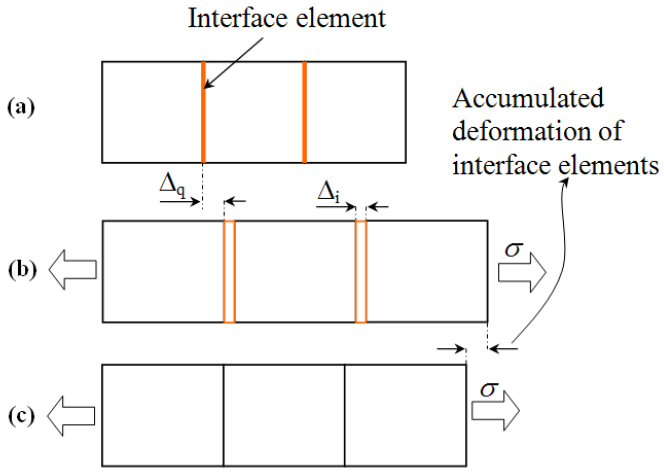

Figure 2. (a) Typical un-loaded 90^o layer specimen, (b) loaded specimen modeled with cohesive elements, (c) original loaded ply specimen with no cohesive elements

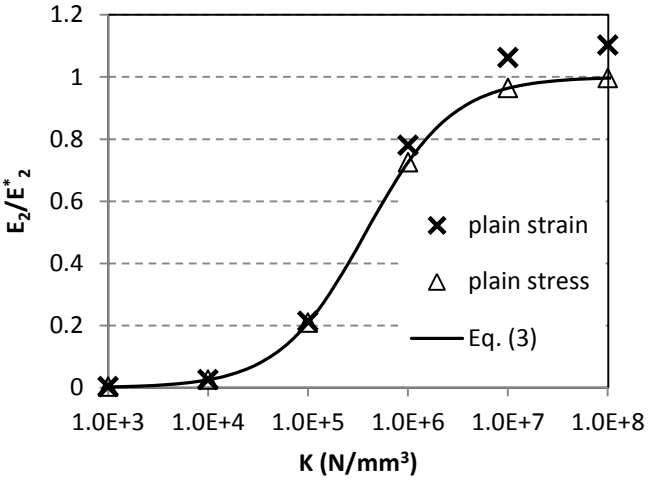

Figure 3. Stiffness ratio versus penalty stiffness value of a uniaxial 90^o ply with m=256, L=6.4 mm and E^*_2=9.6E3 MPa

2-3) Damage initiation and propagation in cohesive elements

In the proposed method, damage growth is modeled by deterioration of cohesive elements while quadrilateral elements behave completely elastic. The conventional bilinear constitutive law is used for cohesive elements for both delamination and matrix crack modeling. The present formulation is a modification of the available bilinear cohesive constitutive law in [26].

The quadratic criterion is used to distinguish the elastic or elastic-damage behavior as follows:

$$F = \sqrt{\left(\frac{<\sigma_1>^+}{T}\right)^2 + \left(\frac{\sigma_2}{S}\right)^2} - (1-\lambda) = 0 \tag{4}$$

where σ_i (i=1 and 2) are stress components in cohesive elements and also S and T are shear and tensile elastic limit stress of the cohesive elements respectively. λ is an internal variable which determines the shrinkage of damage surface by increasing of deformation. The compressive normal stress cannot drive interlaminar damage so when normal stress is negative ($\sigma_1 < 0$), its collaboration in damage is ignored by the symbol $< >^+$ in Equation (4) and is defined in the Equation (5).

$$< x >^+ = \begin{cases} x & if \ \ x > 0 \\ 0 & if \ \ x \le 0 \end{cases} \tag{5}$$

The cohesive element behaves elastically if $F \le 0$ and damage grows if $F > 0$. For delamination growth in mixed mode condition, the power law criterion is used as follows:

$$\sqrt{\left(\frac{G_I}{G_{IC}}\right)^2 + \left(\frac{G_{II}}{G_{IIC}}\right)^2} \ge 1 \tag{6}$$

where G_I, G_{II}, G_{IC} and G_{IIC} are energy release rate of mode I and mode II, and critical energy release rate of mode I and mode II respectively. Figure 4(a) shows pure mode I, II and mixed-mode bilinear constitutive laws of cohesive elements, where $\beta = \Delta_{II}/\Delta_I$, and $\bar{\sigma} = \sqrt{\left(\frac{<\sigma_1>^+}{T}\right)^2 + \left(\frac{\sigma_2}{S}\right)^2}$ is a dimensionless equivalent stress. Figure 4(b) shows the variation of equivalent stress, $\bar{\sigma}$, versus deformation, Δ, for the cohesive element at mixed-mode condition. At an arbitrary point on damage surface like A, the equivalent deformation is Δ and damage shrinkage is determined by internal variable of λ as shown in Figs 4(b).

To have a bilinear softening cohesive law such as one shown in Figure 4(b), λ is set to increase linearly with increasing the value of Δ. More details of formulations are available in [26]. Finally, damage variable, D, on the cohesive element is related to the deformation parameter, Δ, as presented in Equation (7). This formulation [26] is a simple and non-differential one which decrease the error in linearization of the equations and numerical integration.

$$D = \frac{\Delta_F(\Delta - \Delta_0)}{\Delta(\Delta_F - \Delta_0)} \tag{7}$$

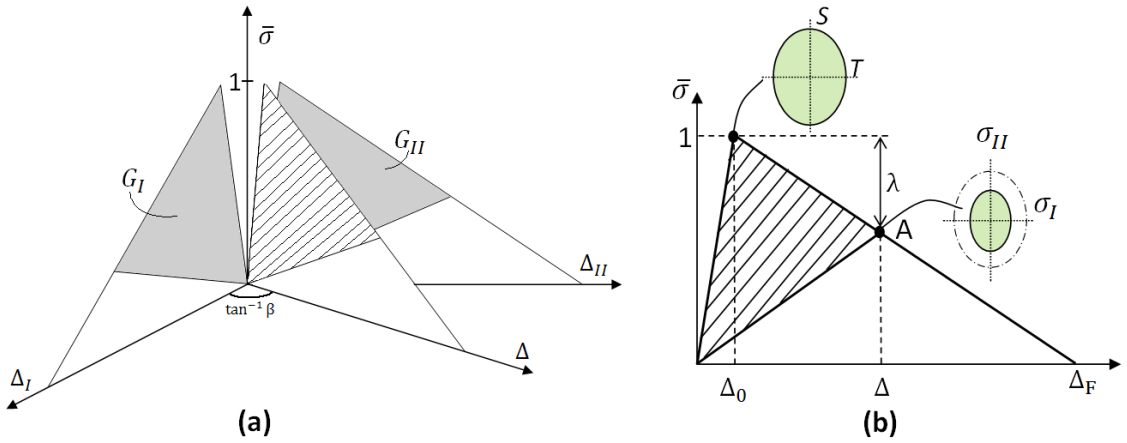

Figure 4 (a) mode I, II and mixed-mode bilinear constitutive laws, (b) shrinkage of damage surface and internal variable λ in mixed-mode condition

2-4) Modeling of Matrix Cracking

Matrix cracking may occur at any point along the 90˚ layers of a cross-ply laminate under tension loading and therefore between any two adjacent rows of quadrilateral elements in the proposed FEM modeling. However, this does not mean that the crack should initiate and propagate at all of the considered series of cohesive elements at each load step. In reality, cracks occur at unknown locations by increasing of loading value. The discontinuous and diffuse natures of transverse cracking seem to be in opposition if not managed properly.
In the present arrangement of cohesive and quadrilateral elements shown in Figure 1(b), if the same material properties are used for all cohesive elements, most of cohesive elements rows experience simultaneous deterioration due to the lack of significant stress gradient in cross-ply specimen under tension. This is however in contradiction with what physically occurs as shown schematically in Figure 1 (a). In other words, if the entire cohesive elements rows use similar values of material properties (i.e. *T*, *S*, G_{IC} , G_{IIC} and K), Equation (4) is satisfied for most of them at almost the same load step and damage variables of elements grows almost similarly. Minor differences may be due to the existence of little stress variation at interface rows and computational error as well. However, in experiment, when a crack initiates and grows at 90˚ layers the normal stress at surrounding material vanishes and no matrix cracking tends to initiate at very close to that. To overcome such a difficulty, two different techniques of "*bisecting*" and "*random distribution of elastic limit*" are examined in this study. To simplify addressing of the second technique, we use "*random*" method hereafter.

2-4-1) Bisecting technique

In this technique, a priority of damage growth is granted to the cohesive elements at the middle of two matrix cracks. Therefore, for a specimen under tension loading with the length of *L* and two cracks at the both ends, the first matrix crack occurs at *x=L/2*, and therefore the

cohesive elements behave elastically except those at the middle of specimen. After crack initiation and propagation at the middle of specimen, the second stage of matrix cracking can occur at $x=L/4$ and at $x=3L/4$ in the same load step. If the cracks at these new locations initiate and propagate through the thickness of the 90º layers, then the behavior of cohesive elements at x=L/8, 3L/8, 5L/8 and 7L/8 are changed from elastic to damageable condition in the same load step. This procedure of increasing the matrix cracks continues until that no more matrix cracking criterion is satisfied, meaning that progressive damage analyses has been converged at a specific load step. In this technique, since the distance between the matrix cracks is always halved, it is called "bisecting" method.

Figure 5 shows a typical specimen with 16 rows of quadrilateral elements as representative of 90˚ layers and 15 rows of cohesive elements, meaning that 15 matrix cracks can take place along the length of that. However, matrix cracking may not necessarily pass all of the predefined cohesive elements rows due to suppressing of the stresses in 90˚ layers and activation of other damage mechanisms such as delamination.

In the elastic damage analysis of this specimen, the priority of cracking occurrence implemented for different rows as explained above. This procedure is repeated for several load steps up to a final load.

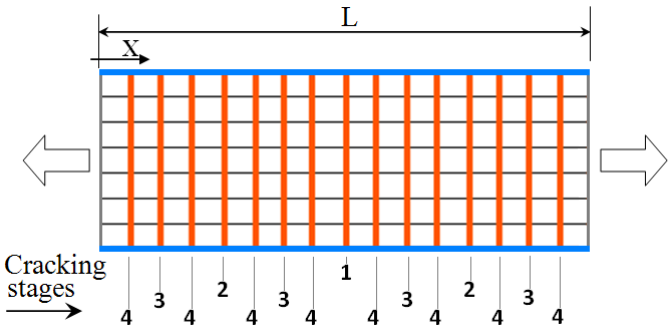

Figure 5. Predefined cohesive elements (thick lines) for a typical speciemen used in bisecting method

2-4-2) Random technique

Another technique to overcome the difficulty of simultaneous damage growth in defined cohesive element rows is a random distribution of material properties for cohesive elements. In this paper, the penalty stiffness and critical energy release rates in mode I and II of all cohesive elements are assumed to be identical but the tensile elastic-limit (T) of cohesive elements in Equation (4) for modeling of matrix-cracking is assumed to be different in various cohesive element rows (randomly selected). By this assumption, damage can initiate and grow randomly in various cohesive elements rows. The Weibull distribution [13] is used for the random distribution of tensile strength, T of cohesive element rows as shown in Equation (8).

$$T = T_0 \left[\ln \frac{1}{1-\eta} \right]^{\frac{1}{m'}} \qquad (8)$$

Where T_0 and m' are scale and shape parameters of the Weibull distribution and they should be obtained from fitting the experimental results to the Weibull distribution. Also η is a random variable between 0 and 1. In a series produced by Weibull distribution (Equation (8)), the average value is quite close to T_0 while m' controls the standard deviation of the data distribution from average value.

When the elastic limit of neighboring cohesive element rows is different, damage initiates earlier in weaker rows. Due to the assumed softening behavior of the cohesive elements, any increase in strain causes more stress relief in the damaged element and therefore, the stress in surrounding elements do not reach their own elastic tensile limit (T). In reality, first transverse cracks appear at weaker locations and stress in nearby material of 90˚ layers is suppressed so this technique is quite similar to what happens in the reality.

3) Results and discussion

To show the capability of this method, three different groups of cross-ply laminates are considered for progressive damage analyses. The computational tool employed for the solution of these problems is a home-built code of nonlinear implicit FEM. This code includes different type of elements, linear and non-linear material properties, and different ways of loading applications, which have been validated for various examples such as delamination growth of composite laminates using cohesive elements within the last 5 years in our university [27-29]. For updating the global stiffness matrix, modified secant method with 50 non-updated iterations was used and found that it is between three to five times faster than the updating complete global matrix in each iteration. Additionally, using secant way assures us to have always positive definite global matrix. For the solution of these problems, Cholesky decomposition technique matched with the Skyline method was chosen and decomposition procedure was just performed in the iterations in which global stiffness matrix was updated. The Newton-Raphson method was not used due to the probability of load drop and non-positive definite global stiffness matrix. Therefore the solution time was longer but it was guaranteed to get a convergence solution.

3-1) $[0/90_3]_s$ laminate

In this section, the selected $[0/90_3]_s$ E-Glass laminate in experimental work reported in [30] is considered for the analyses. The material properties of this laminate are listed in Table 1 [30-31]. Since the value of G_{IIc} was not reported in the original references [30-31], a value of G_{IIc}=0.34 N/mm was assumed in which no induced delamination by transverse cracking occurs because such a damage mode was not reported experimentally. Using symmetry condition along the thickness direction, half of the specimen was modeled only. Crack propagation in general

symmetric laminates is not necessarily a symmetric phenomenon, however in cross-ply laminates, transverse cracks occur perpendicular to the loading directions and after cracks formation, the damaged laminate becomes symmetric with respect to the mid-plane.

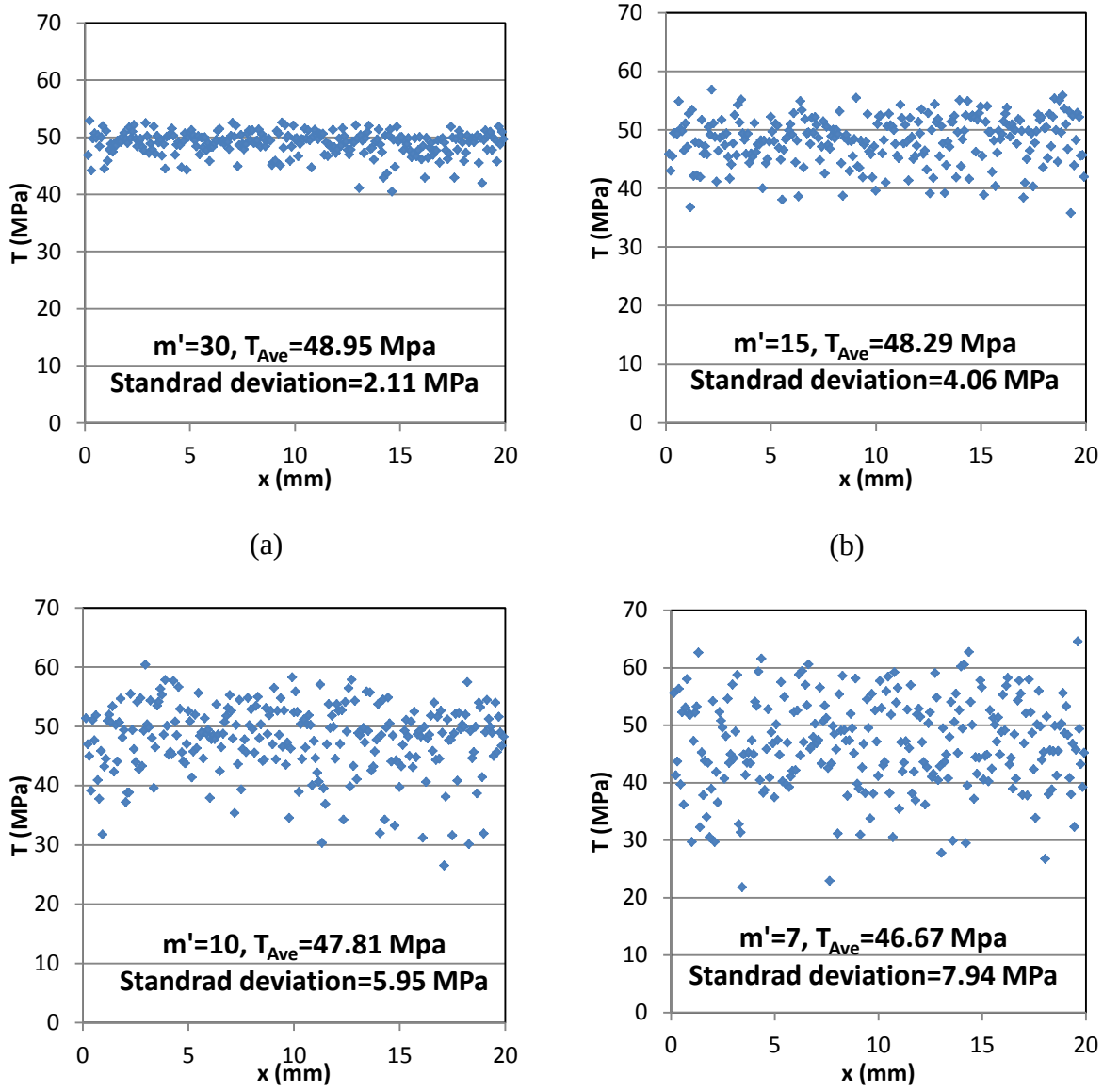

Figure 6. Distribution of T for different cohesive element rows along the specimen (a) $m' = 30$ (b) $m' = 15$ (c) $m' = 10$ (d) $m' = 7$

The length of the model is L=20 mm and three elements per each ply thickness were used. The model was built with 256 parallel rows of identical 8-node quadrilateral elements for modeling 0˚ and 90˚ layers in the length direction, 255 rows of 6-node cohesive elements between 90˚ layers elements for transverse crack modeling and one row of cohesive element at the interface of 0˚ and 90˚ layers. From the experimental results[30], it is known that the average crack spacing would be more than 1.25 mm. So by selecting the mentioned parameters, averagely 16 rows of quadrilateral elements would exist between two transverse

cracks at the largest load level. This number of elements seems enough to capture the stress/strain field properly. The elastic stress limit of the cohesive elements were assumed in the shear yield stress range of typical resin $T = T_0$=50 MPa, and S=75 MPa. It is worth to note that the elastic stress limits do not affect the crack propagation and only affect the damage initiation phase[25, 32]. The penalty stiffness of the cohesive elements was also assumed to be K=1.0E7 N/mm^3 according to the section 2-2.

Table 1. Mechanical properties of E-Glass ply used for $[0/90_3]_s$ laminate [30-31]

E_1	41.7 GPa
E_2	13.0 GPa
ν_{12}	0.30
G_{12}	4.79 GPa
G_{IC}	0.24 N/mm
G_{IIC} (assumed value)	0.34 N/mm
Ply thickness	0.203 mm

To study the effect of randomness, four different distribution of tensile elastic limit with similar T_0 but different m' was selected as shown in Figure 6 over the length of specimen.

The values of T_{Ave} (average T values of each series) of all four specimens are between 48.95 and 46.67 MPa showing less than 5% difference, but the standard deviations of them vary between 2.11 and 7.94. To ensure that neighboring cohesive rows do not experience simultaneous damage initiation in a load step, especially for laminate properties with small standard deviation, very small constant-size load steps was chosen. Loading is considered in a displacement-control manner up to longitudinal strain value of 1.5% and strain increase in each load step is equal to 0.00385% in damaging load increments. Larger loading steps are used in the bisecting method due to the application of cracking stage concept which assures no simultaneous damage growth in neighboring cohesive elements (see Figure 5).

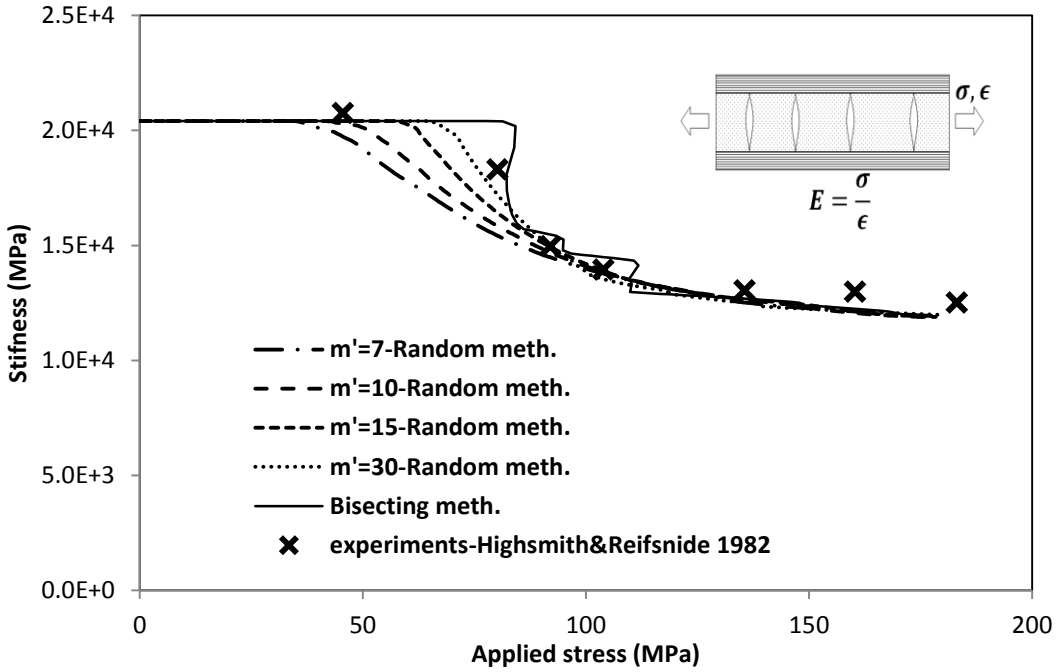

Figure 7. Longitudinal stiffness of $[0/90_3]_s$ E-Glass laminate versus applied stress

Variations of laminate longitudinal stiffness vs. applied stress are depicted in Figure 7 for four elastic limit distribution solved with random and bisecting techniques to be compared with available experimental results from [30]. As expected, stiffness reduction interpreting as damage initiation and propagation, starts earlier in the model with largest standard deviation ($m' = 7$). Increasing the value of standard deviation of T postpones the stiffness reduction or damage initiation. However, among the presented results in this figure, the latest damage initiation occurs for bisecting technique and it is along with a rapid stiffness drop. The predicted stiffness of all models get close to each other at larger applied stress and converges to each other. Figure 7 also shows that the predicted stiffness by all models are quite close to each other and they are in good agreement with experimental results except at the initiation phase of transverse cracking or small values of applied stress. In general, the predicted results by random technique with standard deviation of 2.11MPa ($m' = 30$) are in better agreement with the experimental results. It is worth to mention that sudden stiffness drop in bisecting method is reasonable because while the stress in 90˚ layers does not reach T=50 MPa, no damage initiates in cohesive elements. However, when normal stress exceeds T, because of the high tendency of the specimen to release strain energy, cracking stages as shown schematically in Figure 5 occur one by one which causes large stiffness drop.

Slight snap-backs can also be seen in the curve of bisecting method which is due to small stress drop in rapid transverse cracking. Since the problem is solved in a displacement-control manner, it is possible to capture load drops. Therefore, the bisecting curve of stiffness versus applied stress has small turnings to the stress direction.

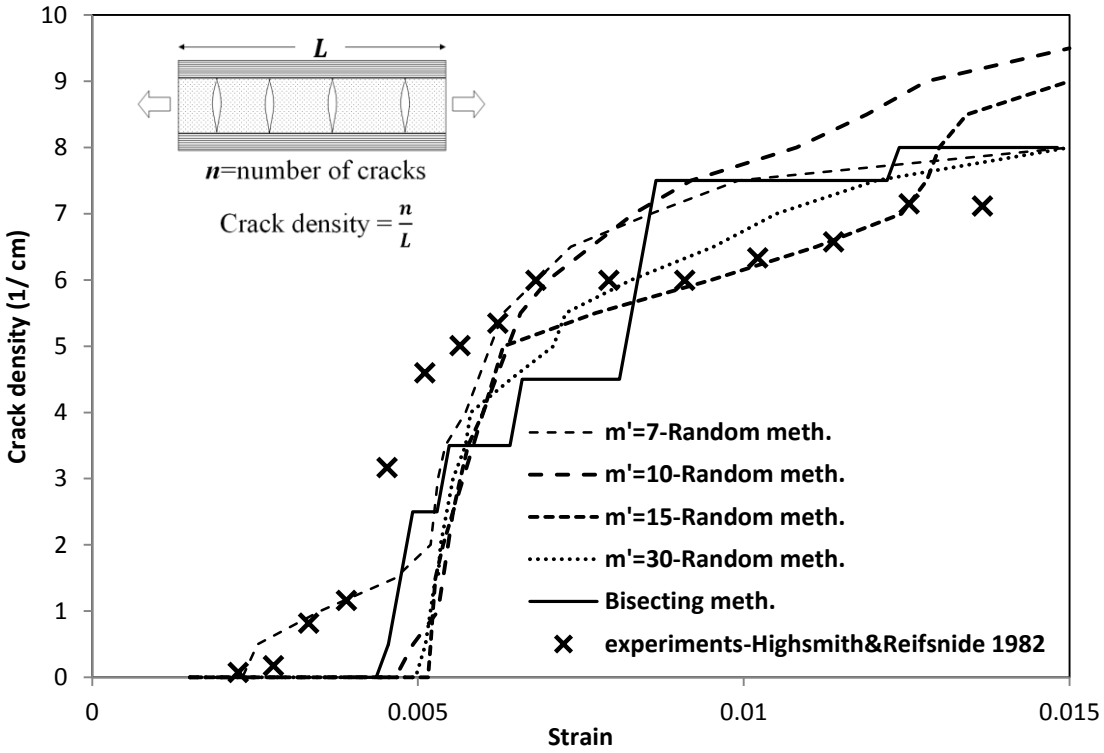

Figure 8. Crack density versus applied strain for $[0/90_3]_s$ E-Glass laminate

It was observed that in random technique, transverse cracks do not catastrophically expand over whole thickness of 90˚layers. This fact make a bit hard to count the number of cracks exactly and to find the crack density in a laminate especially in initiation phase. However, it does not affect the validity of solution procedure because by applying a very small load step, after damage initiation in a cohesive element row, normal stresses relaxes and therefore neighboring rows would not experience any damage. In bisecting method, crack initiation and expansion to whole thickness of 90˚ layers was in the same load step so counting the number of matrix cracking is easier. Figure 8 shows the variations of crack density versus applied strain of different techniques and compare with experimental results. For random technique, a transverse crack is counted when the cohesive elements attached to the interface of 0˚ and 90˚ layers start to deteriorate. The obtained results from random technique indicate that, damage initiates earlier in the laminates with large value of standard deviation of T ($m' = 7$). The transverse crack appearance in bisecting method is in between the results of random models. This seems to be in contradiction with the results in Figure 7. However, it should be explained that in drawing Figure 8, while a transverse crack do not grow through the complete thickness of 90˚ layers, it was not counted. This means that damage may initiate in a cohesive element row and therefore affect the total stiffness of the laminate but while it is not completed, it is not counted. In other words, Figure 7 and Figure 8 are indications of different aspects of diffuse damage in 90˚ layers. Figure 7 shows the overall effect of cohesive element damage on laminate stiffness while Figure 8 shows the number of completed matrix cracks in different load step.

The predicted crack densities from both techniques are not far from the experimental results, but the results of random model with $m' = 30$ and bisecting method are in better agreement with the experimental results. It is worth to note that the results such as crack density versus applied strain usually contains scattering even for experiments only and is not a precisely repeatable result.

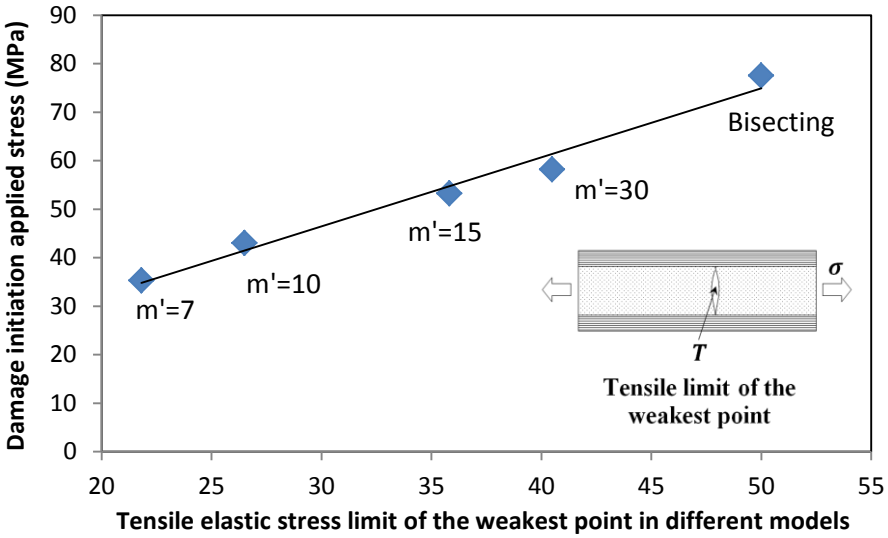

Figure 9. Damage initiation stress of $[0/90_3]_s$ E-Glass laminate versus elastic tensile limit of the weakest point

Damage initiation stress of different models is shown versus the elastic tensile limit of the weakest point in Figure 9. Since in bisecting technique, the elastic limit of all cohesive elements is the same, T=50 MPa is assumed for the weakest point of the laminate. Figure 9 indicates that the damage initiation stress is proportional with the elastic stress limit of the weakest point of the laminate. The main reason of variation of strength of different point in a laminate is related to the distribution and amount of defects so this figure shows as the volume of the imperfections is reduced over the specimen, the damage initiation stress increases. Furthermore, the bisecting technique can properly show the upper limit of damage initiation stress as an idealized material with no imperfection.

3-2) $[90_n/0]_s$ laminates

In this section, transverse cracking and delamination of cross-ply laminates with $[90_n/0]_s$ (n=1,2,3) layups are analyzed. The material properties of the specimens are listed in

Table **2**. The effective Young's modulus of a ply in 0˚ direction can be also calculated which is E_1=39.7 GPa. Equal size of cohesive elements were selected for both delamination and matrix cracking modeling to eliminate the size effects of cohesive elements on damage initiation and propagation. The length of the specimens is L=6.4 mm and they all include 256 rows of similar quadrilateral elements in the longitudinal, x, direction. Due to the existence of

symmetry conditions along the thickness direction, half of each laminate was modeled in the finite element analyses.

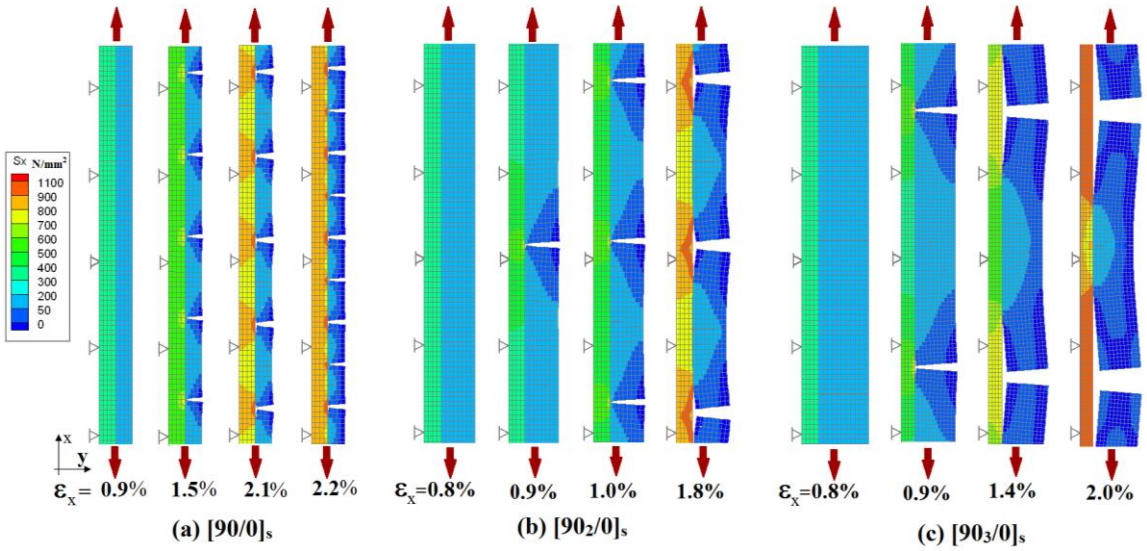

Figure 10. Damage growth prediction using bisecting technique (five times exaggeration in displacement field), (a) $[90/0]_s$, (b) $[90_2/0]_s$, (c) $[90_3/0]_s$

Table 2. Mechanical properties of a GFRP ply [13]

Fiber Young's modulus, E_f	76 GPa
Fiber volume fraction	0.50
Matrix Young's modulus, E_m	3.4 GPa
Poisson's ratio of the matrix, ν_m	0.35
Young's modulus of the 90˚ ply, E_2	9.6 GPa
Poisson's ratio of the 90˚ ply ν_{90}	0.31
Critical Energy release rate-mode I	0.15 N/mm
Critical Energy release rate-mode II	0.30 N/mm
Ply thickness	90 μm
E_1 (calculated by rule of mixture)	39.7 GPa

The penalty stiffness of K=1.0E7 N/mm was considered for all cohesive elements in different models. The value of the tensile strength of matrix was assumed to be T=90 N/mm^2 according to [13], and also shear strength of the matrix to be, S=100 N/mm^2. The damage growth procedure of laminates with $[90_n/0]_s$ (n=1,2,3) layups modeled with bisecting technique for an specimen with 2 mm length are illustrated in Figure 10 for four different load steps. The nonlinear solution for each laminate contains 25 load steps with the tensile strain increments of $\Delta\varepsilon_x$=0.1%. For better demonstration of results in this figure, the cohesive elements are not displayed and therefore the cracks are distinguishable.

A uniform matrix crack density can be observed in all loading states, which is due to the implementation of bisecting procedure described in the previous section. At the end of each

load step, one or more cracking stages may occur. It can be seen for n=2 and n=3 damage mode changes from transverse cracks accumulation to induced delamination after a certain crack density known as critical crack density. Delamination grows after the saturation of matrix crack density for these layups. Figure 10 also shows that the saturation crack density decreases with increasing the number of 90^o layers.

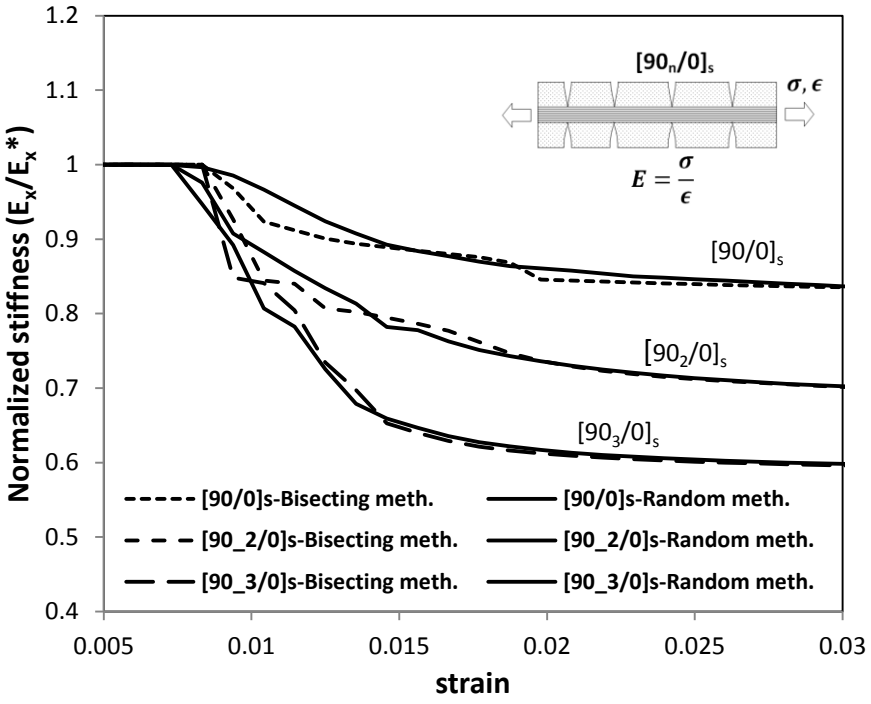

Figure 11. Reduced stiffness ratio versus applied strain for $[90_n/0]_s$ (n=1,2,3) laminates

Figure 11 shows the normalized stiffness (ratio of longitudinal laminate stiffness, E_x, over the undamaged laminated stiffness E_x^*) versus the applied strain for the concerned laminates. It is clear that by increasing in the thickness of 90˚ layer, the stiffness ratio decreases larger and more rapidly. This shows that the proposed approach could capture the effect of 90˚ layers thickness.

Figure 12 compares the variations of predicted matrix crack density of bisecting method with the available experimental results in [13] up to the applied strain of ε_x=2.0%. This figure shows a good agreement of both predicted matrix crack initiation and saturation densities with the experimental findings for the considered three cross ply laminates. It is worth to note that the experimental results were available up to the applied strain of 1.8% and un-grouped for different laminates.

Delamination was not observed for the laminate with $[90/0]_s$ layup up to the applied strain of ε_x=2.5%, but it was observed for $[90_2/0]_s$ and $[90_3/0]_s$ laminates when the matrix crack density reaches a certain value (critical crack density). Comparing the presented results in Figure 11 and Figure 12, it is clear that induced delamination affects the stiffness decrease of $[90_2/0]_s$ and $[90_3/0]_s$ laminates significantly. For instance laminate $[90_3/0]_s$ has constant transverse crack density between two states of ε_x=0.9% and ε_x=1.4% as can be seen from Figure 10, but according to Figure 11 it experience a large stiffness reduction due to induced

delamination. This stiffness decrease is more significant in laminates with larger number of 90˚ layers.

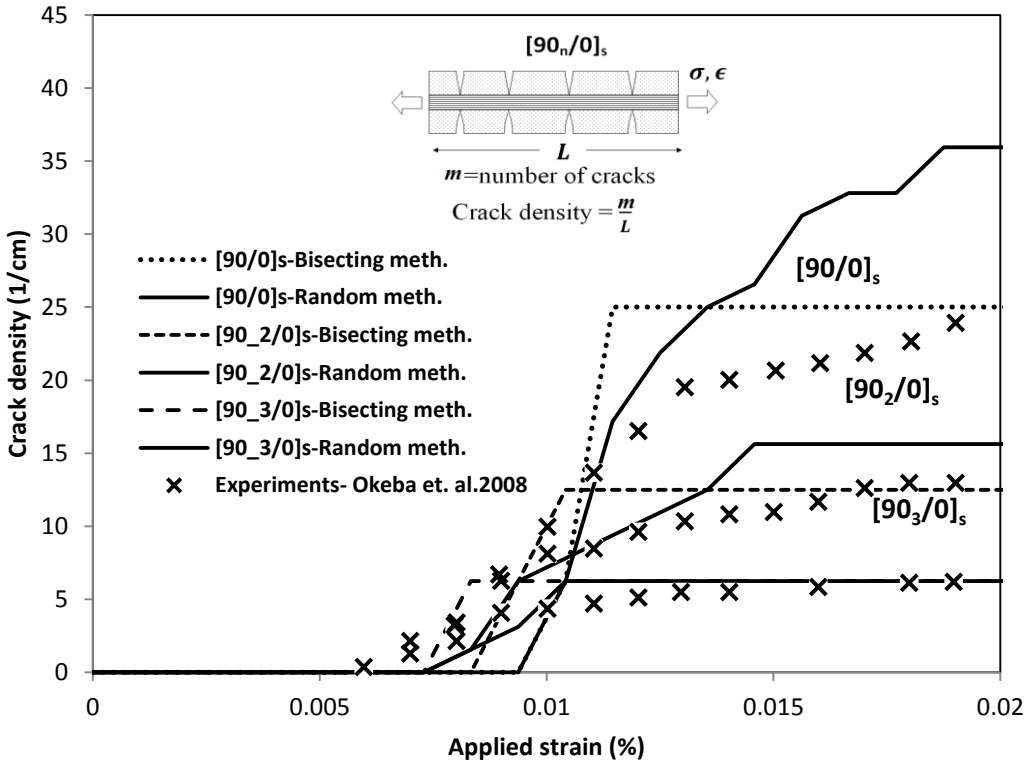

Figure 12. Matrix crack density versus applied strain for $[90_n/0]_s$ (n=1,2,3) laminates using bisecting method

For implementation of random technique, the penalty stiffness value and material properties except the elastic-limit of stress are selected to be similar to the values used in the bisecting technique. Equation (8) is used to define a proper distribution of elastic normal limit and according to [13], it was assumed that $m' = 15$, and $T_0 = 105 MPa$. Figure 13 shows the damage growth of laminates with $[90_n/0]_s$ (n=1,2,3) layups for a part of the specimen with the length of about 2 mm. The crack spacing is not necessarily uniform and therefore, delamination length is not identical for all of matrix cracks. It was observed that delamination initiation and growth are the consequences of matrix cracking saturation and this is in agreement with many experimental findings as indicated in [5, 8, 14]. Similar to bisecting method, the critical crack density is decreased with increasing the number of 90^o layers.

The obtained reduced stiffness ratio of the lay-ups are very close to the results of bisecting method as shown in Figure 11. Similar to bisecting method, lay-ups with thicker 90˚ layers experience larger stiffness drop. Similar to the results shown in last section for specimen of $[0/90_3]_s$, stiffness reduction starts earlier in random method but as strain value becomes larger, the result of both techniques become closer to each other.

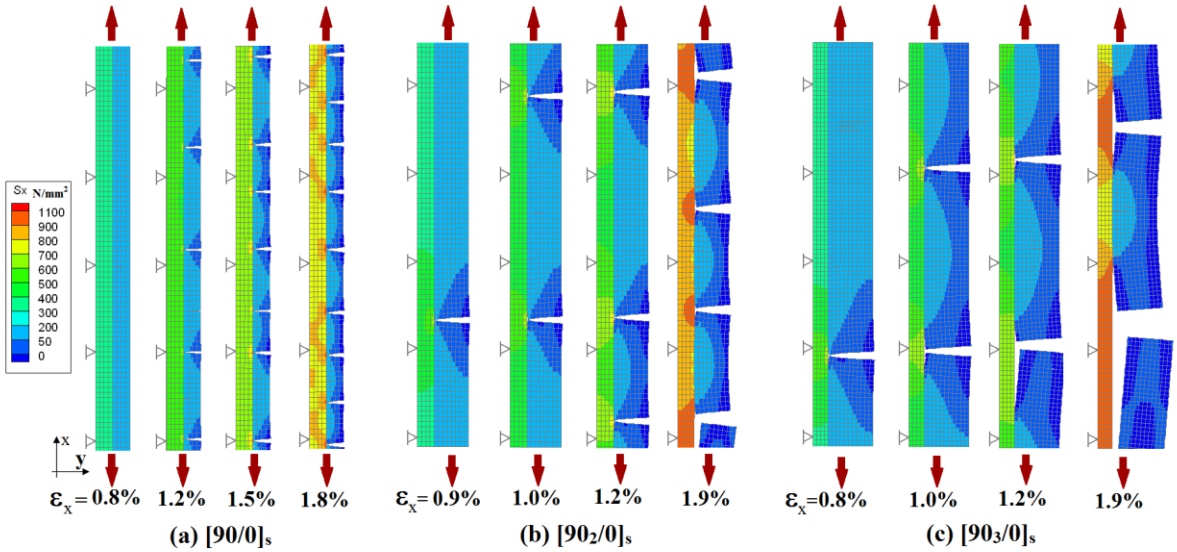

Figure 13. Damage growth prediction using random technique (five times exaggeration in displacement field), (a) $[90/0]_s$, (b) $[90_2/0]_s$ and (c) $[90_3/0]_s$

The obtained matrix crack density versus applied strain from the random technique is also demonstrated in Figure 12. The obtained results of this method for $[90_2/0]_s$ and $[90_3/0]_s$ laminates are in good agreement with the experimental results. The obtained values of crack densities for the $[90/0]_s$ laminate are significantly larger than the experimental results for the remote strains of larger than 1.2% which can be due to the strong dependency of damage procedure of this laminate on random material properties of the parallel cohesive element rows. The thickness of 90˚ layer in this lay-up is just 90μm which is very thin and delamination does not play a significant role for $[90/0]_s$ laminate and the total damage procedure is determined by the randomly distributed material properties and matrix cracking phenomena. Therefore, the obtained results may be improved by more precise description of material randomness and finer mesh in this particular case.

3-3) $[90_n/0]$ asymmetric cross-ply laminates

In this section, matrix cracking and delamination analyses are performed for asymmetric cross-ply laminates using both bisecting and random distribution of cohesive elements material properties techniques. For this purpose, three laminates with the lay-ups of $[90_n/0]$ (n=1, 2, 3) are modeled. To the best knowledge of the authors, no analytical solution has been already performed for such asymmetric laminates. The lay-up asymmetry condition causes stress variation along the thickness direction of laminates leading to a significant effect on progressive damage of them. The material properties of the used laminates are considered to be the same as those in
Table **2**. For boundary conditions, no constraint is applied to the specimen over the length except the ends where all of the nodes are restricted in longitudinal direction.

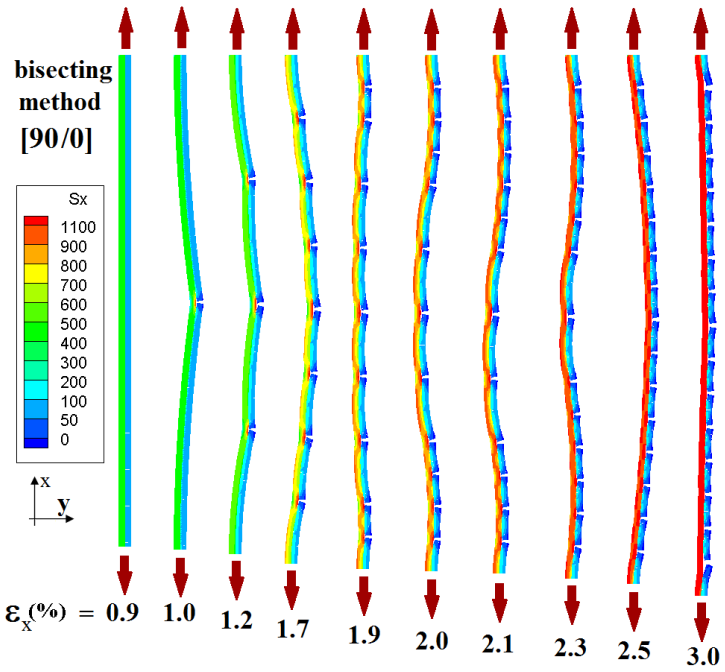

Figure 14. Damage growth of [90/0] laminate for various applied strains using bisecting technique (five times exaggeration in displacement field)

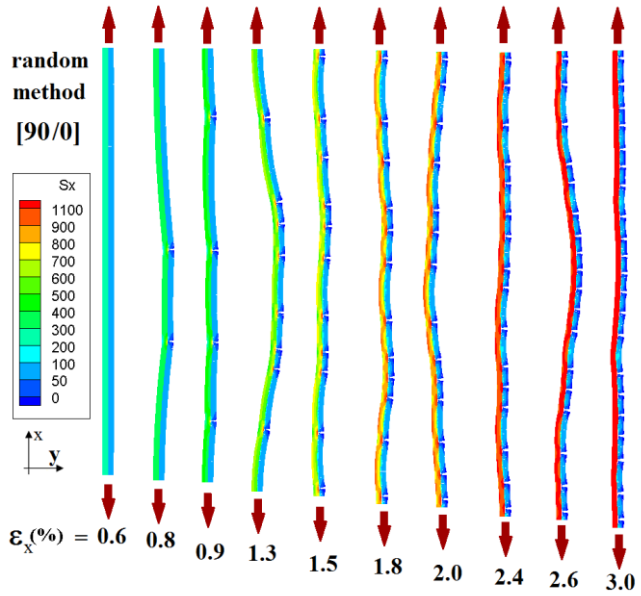

Figure 15. Damage growth of [90/0] laminate for various applied strains using random distribution of elastic limit (five times exaggeration in displacement field)

Matrix cracking and induced delamination analyses were also performed for $[90_2/0]$ and $[90_3/0]$ laminates using both bisecting and random techniques. The obtained results are shown in Figure 16 for $[90_2/0]$ and Figure 17 for $[90_3/0]$. These figures show that the first matrix cracking incidence in these laminates is rapidly followed by delamination initiation in both methods. Any load increase after this phenomenon causes the growth of interlaminar cracks and no more matrix cracking within the 90˚ layers. One reason for this behavior is the

existence of compressive stresses in the outer fibers of 90˚ layers due to the partially bending in the specimen. Any load augmentation, causes increase in the curvature, the local bending value and therefore the larger compressive stress. It is also clear that the damage behavior of these laminates is completely different from the lay-up of [90/0].

Damage initiation in both laminates of $[90_2/0]$ and $[90_3/0]$ with the same solution technique occurs at almost same applied strain (0.8% for bisecting and 0.7% for random techniques). It can be also concluded that the obtained progressive damage results from both techniques are very close and sound in agreement with each other considering the fact that there exist some weaker cohesive elements in the random technique.

For more comparison of the obtained results for various asymmetric laminates and solution techniques, the effective external remote stress of the asymmetric laminates versus applied strain are shown in Figure 18. The obtained general stress-strain behaviors of each laminate from different techniques are almost similar except the point of damage initiation, which was discussed before for symmetric laminates.

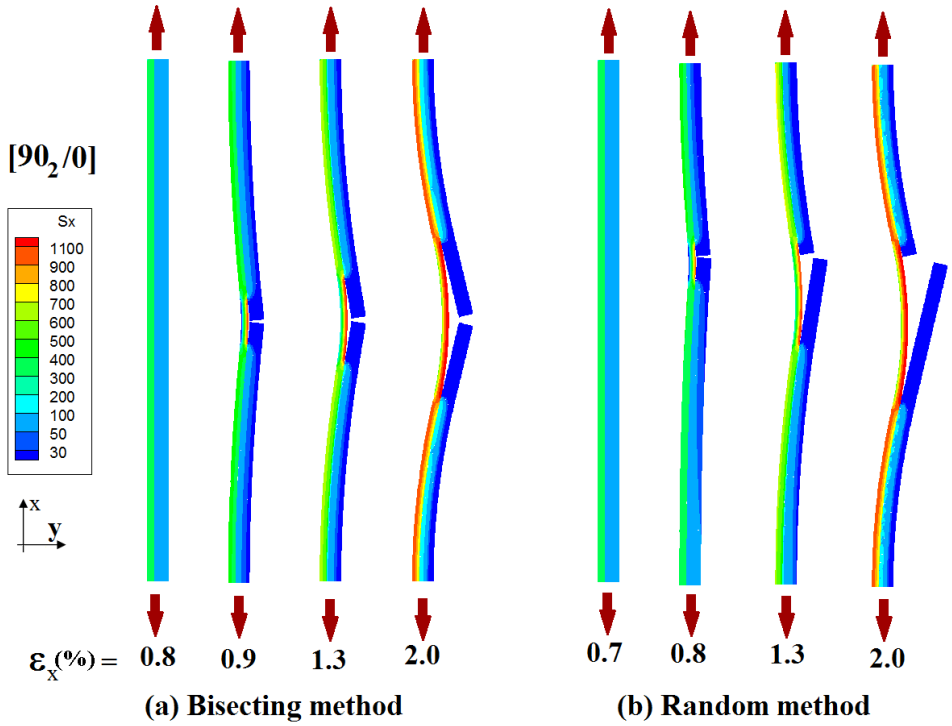

Figure 16. Damage growth of $[90_2/0]$ laminate, (a) bisecting technique, (b) random distribution of elastic limit

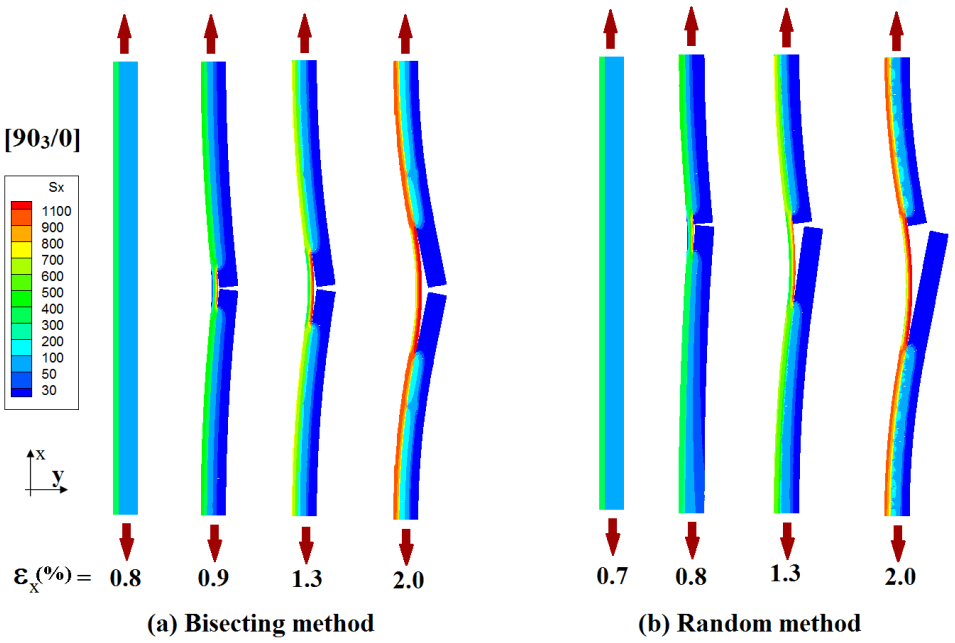

Figure 17. Damage growth of [90_3/0] laminate, (a) bisecting technique, (b) random distribution of elastic limit

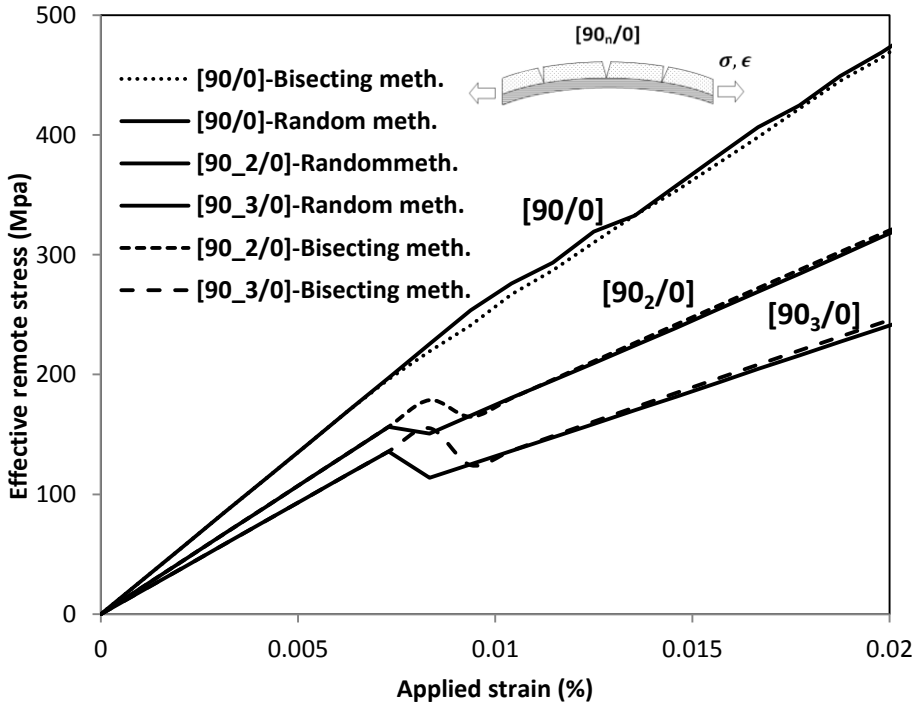

Figure 18. Effective remote stress versus applied strain for various asymmetric laminates within damage growth

Damage initiation and propagation of [90/0] laminate for various applied strain were obtained and depicted in Figure 14 and Figure 15 using bisecting and random techniques respectively. In these figures, the left side part of each plot shows the 0˚ ply and the right side belongs to

the 90˚ ply. These figures show that the stress level of the 0˚ layer is always larger than the 90˚ layer and the matrix crack density is gradually increased in the 90˚ layer by increasing the applied strain. The obtained matrix crack density remained almost unchanged for the applied strain of larger than 2.5%. Figure 14 and Figure 15 also show that matrix cracking causes out of plane displacement in laminates with asymmetric lay-ups while applying in-plane tensile loading. The obtained out of plane behaviors from both techniques are almost similar. Except very near the ends of specimens modeled by bisecting method and at strain of 3.0%, no induced delamination observed. It is noted that the displacement values in these figures are also displayed with five times exaggeration for better presentation of results.

4) Conclusion

In this paper, two techniques of bisecting and random distribution of elastic stress limit were examined for modeling of initiation and propagation of matrix cracking and induced delamination in symmetric and asymmetric cross-ply laminates. The first damage mode is accumulation of transverse cracking and after a certain value of crack density known as crack density saturation, the damage mode changes to delamination at the tips of transverse cracks. Transverse cracking is independent of shear toughness G_{IIc} up to saturation crack density which can be known as an upper limit of transverse cracking in a certain laminate. Delamination initiation (saturation crack density) depends on different parameters such as stiffness of 0° and 90° layers, G_{IIc}, and 90° layers thickness, so transverse cracking can be restricted by the combination of mentioned parameters.

The obtained results of damage growth, laminate stiffness and crack density versus applied strain from both techniques were generally in agreement with the available experimental results. The obtained results from both techniques were also in a very good agreement with each other for both symmetric and asymmetric laminates. The performed analyses for asymmetric cross-ply laminates of $[90_n/0]$ (n=1 to 3) showed the capability of this method in progressive damage analyses of composite laminates. The proposed method is less restricted in comparison with available micromechanical methods and is able to predict damage initiation, propagation and damage-mode transition for any symmetric and asymmetric cross-ply laminate. Therefore, this method can be used for development of “in-plane damage” constitutive laws especially when specimens are subjected to complex loading and boundary conditions.

References

1. O'brien TK. Analysis of Local Delamination and their Influence on Composite Laminate Behavior. In: Johnson WS, (ed.). *Delamination and Debonding of Materials, ASTM STP 876*. American Society for Testing and Materials, 1985, p. 282–97.
2. Farrokhabadi A, Hosseini-Toudeshky H and Mohammadi B. A generalized micromechanical approach for the analysis of transverse crack and induced delamination in composite laminates. *Compos Struct*. 2011; 93: 443-55.
3. Garrett KW and Bailey JE. Multiple transverse fracture in 908 cross-ply laminates of a glass fiber reinforced polyester. *Journal of Materials Science*. 1977; 12: 157–68.
4. Fukunaga H, Chou T-W, Peters PWM and Schulte K. Probabilistic failure strength analyses of graphite/epoxy cross-ply laminates. *J Compos Mater*. 1984; 18: 339-56.
5. Takeda N and Ogihara S. Initiation and growth of delamination from the tips of transverse cracks in CFRP cross-ply laminates. *Compos Sci Technol*. 1994; 52: 309-18.
6. Berthelot JM and Le Corre JF. A model for transverse cracking and delamination in cross-ply laminates. *Compos Sci Technol*. 2000; 60: 1055-66.
7. Hashin Z. Analysis of cracked laminates: a variational approach. *Mech Mater*. 1985; 4: 121-36.
8. Nairn JA and Hu S. The Initiation and Growth of Delamination Induced by Matrix Microcracks in laminated Composites. *International Journal of Fracture*. 1992; 57: 1-24.
9. Zhang H and Minnetyan L. Variational analysis of transverse cracking and local delamination in [[theta]m/90n]s laminates. *International Journal of Solids and Structures*. 2006; 43: 7061-81.
10. Silberschmidt VV. Matrix cracking in cross-ply laminates: effect of randomness. *Composites Part A: Applied Science and Manufacturing*. 2005; 36: 129-35.
11. Andersons J, Joffe R and Sparnins E. Statistical model of the transverse ply cracking in cross-ply laminates by strength and fracture toughness based failure criteria. *Engineering Fracture Mechanics*. 2008; 75: 2651-65.
12. Maimı´ P, Camanho PP, Mayugo JA and Turon A. Matrix cracking and delamination in laminated composites. Part I: Ply constitutive law, first ply failure and onset of delamination. *Mech Mater*. 2011; 43: 169-85.
13. Okabe T, Nishikawa M and Takeda N. Numerical modeling of progressive damage in fiber reinforced plastic cross-ply laminates. *Compos Sci Technol*. 2008; 68: 2282-9.
14. Boniface L, Smith PA, Bader, M. G. and Rezaifard AH. Transverse Ply Cracking in Cross-Ply CFRP Laminates--Initiation or Propagation Controlled? *J Compos Mater*. 1997; 31: 1080-112.
15. Liu PF and Zheng JY. Recent developments on damage modeling and finite element analysis for composite laminates: A review. *Materials & Design*. 2010; 31: 3825-34.
16. Barbero EJ and Lonetti P. An Inelastic Damage Model for Fiber Reinforced Laminates. *J Compos Mater*. 2002; 36: 941-62.
17. Bazant ZP and Pijaudier-Cabot G. Nonlocal continuum damage and measurement of characteristic length. *American Society of Mechanical Engineers, Applied Mechanics Division, AMD*. Berkeley, CA, USA: Publ by American Soc of Mechanical Engineers (ASME), 1988, p. 79-85.

18. Kumar RS and Talreja R. A continuum damage model for linear viscoelastic composite materials. *Mech Mater*. 35: 463-80.
19. Allix O and Hild F. Continuum Damage Mechanics of Materials and structures: Present and Future. In: Allix O and Hild F, (eds.). *Continuum Damage Mechanics of Materials and structures*. Elsevier, 2002.
20. Ladevèze P, Lubineau G and Marsal D. Towards a bridge between the micro- and mesomechanics of delamination for laminated composites. *Compos Sci Technol*. 2006; 66: 698-712.
21. Ladevèze P and Nouy A. On a multiscale computational strategy with time and space homogenization for structural mechanics. *Computer Methods in Applied Mechanics and Engineering*. 2003; 192: 3061-87.
22. Soutis C and Beaumont PWR. Multi-scale modelling of composite material systems. Woodhead, 2005.
23. Song J-H and Belytschko T. Multiscale aggregating discontinuities method for micro-macro failure of composites. *Composites Part B: Engineering*. 2009; 40: 417-26.
24. Johnson P and Chang FK. Characterization of Matrix Crack-Induced Laminate Failure—Part I: Experiments. *J Compos Mater*. 2001; 35: 2009-36.
25. de Borst R. Numerical aspects of cohesive-zone models. *Engineering Fracture Mechanics*. 2003; 70: 1743-57.
26. Davila CG, Camanho PP and de Moura MF. Mixed-Mode Decohesion Elements for Analyses of Progressive Delamination. *42nd AIAA/ASME/ASCEIAHS/ASC Structures, Structural Dynamics and Materials Conference*. Seattle, Washington2001, p. Paper AIAA-01-1486.
27. Hosseini-Toudeshky H, Jalalvand M and Ghayour MH. Numerical Aspects of Delamination Modeling Using Interface Elements. *Key Eng Mater*. 2011; 471 - 472: 606-9.
28. Hosseini-Toudeshky H, Jalalvand M and Mohammadi B. Delamination analysis of holed composite laminates using interface elements. *Procedia Engineering*. 2009; 1: 39-42.
29. Jalalvand M. Delamination Analysis of Laminated Composite Material by using Interface Element. *Aerospace Engineering*. Tehran: Amirkabir University of Technology, 2008.
30. Highsmith AL and Reifsnider KL. Stiffness reduction mechanisms in composite laminates. In: Reifsnider KL, (ed.). *Damage in Composite Materials*. ASTM STP, 1982.
31. Lim SG and Hong CS. Effect of transverse cracks on the thermomechanical properties of cross-ply laminated composites. *Compos Sci Technol*. 1989; 34: 145-62.
32. Balzani C and Wagner W. An interface element for the simulation of delamination in unidirectional fiber-reinforced composite laminates. *Engineering Fracture Mechanics*. 2008; 75: 2597-615.

Nomenclature

D: damage variable at cohesive element

E_2^* : longitudinal stiffness of a 90º ply

E_2 : longitudinal stiffness of a 90º ply with embedded m-1 cohesive elements

F: damage initiation criterion

G_I : energy release rate of mode I

G_{II} : energy release rate of mode II

G_{IC} : critical energy release rate of mode I

G_{IIC} : critical energy release rate of mode II

K: penalty stiffness value of the cohesive element

L: length of the specimen

n: number of 90˚ layers in lay-ups

m: number of rows of quadrilateral elements

S: shear elastic stress limit

T: tensile elastic stress limit

T_0: scale parameter of the Weibull distribution

T_{Ave}: average of T in a specimen modeled by random technique

m' : shape parameter of the Weibull distribution

Δ : value of displacement discontinuity vector of Δ_j (j=1 and 2)

Δ_0 : displacement discontinuity of elastic-damage limit

Δ_i : displacement of cohesive elements in normal direction

Δ_j (j=1 and 2) :displacement discontinuity at the cohesive element

Δ_F : displacement discontinuity associated with D=1

Δ_q : displacement of quadrilateral elements

ε_2 : longitudinal strain in 90º ply

η : a random value between 0 and 1

λ : internal variable which determines the shrinkage of damage surface

σ_j (j=1 and 2): stress components in cohesive element

σ : longitudinal stress in 90º ply